Simulations numériques versus Benchmarks expérimentaux de la propagation des ondes en environnement topographique complexe : résultats d'une méthode d'éléments finis spectraux et de la méthode de l'intégrale de Kirchhoff discrétisée

N. Favretto-Cristini[a], P. Cristini[a], A. Tantsereva[b], B. Ursin[b], D. Komatitsch[a] et A.M. Aizenberg[c]

[a]CNRS, Laboratoire de Mécanique et d'Acoustique UPR 7051, 31 chemin Joseph Aiguier, 13402 Marseille Cedex 20, France

[b]NTNU -Department of Petroleum Engineering and Applied Geophysics, S.P. Andersens vei 15A, N-7491 Trondheim, Norvège

[c]Institute of Petroleum Geology and Geophysics SB RAS, Pr.Ac.Koptyug 3, 630090 Novosibirsk, Fédération de Russie

favretto@lma.cnrs-mrs.fr

Accurate simulation of seismic wave propagation in complex geological structures is widely used for environmental and industrial applications for subsurface structure evaluation and in seismic exploration as a core tool of seismic imaging and inversion methods. However, conventional methods fail to simulate realistic wavefields in geological media with large and rapid structural changes, due to the presence of shadow zones, diffractions and/or edge effects. Different methods have been developed to improve seismic modeling in complex geological environment. They are typically tested either on synthetic configurations against "validated" methods, or via direct comparison with real data acquired *in situ*. Such approaches have limitations, especially if the propagation occurs in a complex environment with strong-contrast reflectors and surface irregularities. An alternative approach for seismics consists in comparing the synthetic data with data obtained in laboratory under controlled conditions for a known configuration. We present here a comparison of laboratory data of 2D and 3D zero-offset wave reflection from a strong topographic environment immersed in a water tank with synthetic data computed by means of a Spectral-Element Method and the Tip-Wave Superposition Method. The results indicate a good fit in time arrivals and amplitudes.

1 Introduction

Accurate simulation of seismic wave propagation in complex geological structures is widely used for environmental and industrial applications for subsurface structure evaluation and in seismic exploration as a core tool of seismic imaging and inversion methods. In models with simple structures and slowly varying material properties, conventional methods (*e.g.*, ray methods, finite-difference methods) are efficient tools. However, difficulties arise for complex geological structures with large and rapid structural changes, and conventional methods fail to simulate realistic wavefields, due essentially to the presence of shadow zones, diffractions, and edge effects. Different methods have thus been developed to improve seismic modeling in complex geological environments with structural complexities like faults with steep dips or curved reflectors. They are typically tested on synthetic configurations against analytical solutions for simple canonical problems or reference methods, and several projects focusing on verification and validation of numerical methods have been conducted in the last few years [11]. Such an approach has limitations, especially if the propagation occurs in a complex environment with strong-contrast reflectors and surface irregularities, as it can be difficult to determine the method which gives the best approximation of the "real" solution given by a reference method. Another approach is to validate these methods via direct comparison with real data acquired *in situ* [9]. Unfortunately, without a priori (good) knowledge of the geological environment, the interpretation of the obtained results may be a tedious task due to the existence of diffraction and sideswipe events.

An alternative approach for seismics consists in comparing the synthetic data with data obtained in the laboratory. In contrast with *in situ* experiments, high-quality data are collected under controlled conditions for a known configuration, which is crucial for comparisons with numerical models. Moreover, unlike synthetic data, laboratory data possess many of the characteristics of field data (random and signal-generated noise, multiples, mode conversions), as real waves propagate through models with no numerical approximations. Our aim is to study 3D complications in zero-offset reflection profiles acquired over a strong topographic environment in order to improve the understanding of the physical mechanisms involved in the interaction of the waves with irregular surfaces. As noted previously, in such a complex environment the numerical methods based on approximations may fail to simulate accurately the seismic wavefields and produce different results depending on their intrinsic hypotheses. The main purpose of this work is therefore to test the approach using laboratory data as reference data for benchmarking 2D and 3D numerical methods and techniques. Using the indoor tank facilities of the Laboratory of Mechanics and Acoustics (LMA, Marseille, France) we have performed laboratory-scaled measurements of zero-offset reflection of broadband pulses on a model containing topographic structures with several edges and corners and immersed in a water tank. The presence of these structures is expected to complicate the wavefields significantly. In what follows we present comparisons of these measurements with numerical data simulated by means of a Spectral-Element Method (SEM) and a Discretized Kirchhoff Integral Method (DKIM).

2 Methods

2.1 Experimental method

We carried out laboratory experiments at Laboratory of Mechanics and Acoustics in Marseille, France. The model used in these experiments, called the "Marseille model", is partly based on French model [7], but contains additional topographies such as a truncated dome and a truncated pyramid (Fig. 1(a)). The model of size 600 x 400 x 70 mm^3 is made of PVC material which is isotropic at ultrasonic frequencies, and whose measured properties are in the same range as those of typical geological media. The thickness of the model varies from 30 to 70 mm, the difference between two levels, separated by a planar fault, being 40 mm. The model was immersed in a water tank which is equipped with a computer-controlled system which allows for accurate positioning of the source and receiver. The measured properties of the materials are $V_P = 1476 - 1493$ m/s (depending on the water temperature), $\rho = 1000$ kg/m^3 in the water layer, and $V_P = 2220$ m/s, $V_S = 1050$ m/s, $\rho = 1412$ kg/m^3 in the PVC material. Attenuation in the PVC layer is described by quality factors $40 < Q_P < 60$ and $27 < Q_S < 31$ for P and S-waves, respectively. Attenuation in the water is negligible. As zero-offset seismic configuration is considered for these experiments, the model is illuminated by a piezoelectric transducer which operates both as a source and a receiver. Different kinds of transducers with a central frequency f_c equal to 500 kHz are used: one transducer with diameter $D = 25.4$ mm and narrow-beam (NB) aperture (about 8° at -3 dB), and one transducer with diameter $D = 3$ mm and broad-beam (BB) aperture (about 45° at −3 dB), which allows us to obtain 3D zero-offset data.

Conventional ultrasonic pulse-echo technique wass used to obtain the reflection data from the Marseille model. The distance from the transducer to the flat part of the model surface is either 105 mm ± 1 mm, or 150 mm ± 1 mm, the far-field condition being thus fulfilled for any position of the transducer. Wave propagation is performed in small-scale conditions, *i.e.*, for instance, if a scale ratio of 2.10^4 is considered an experimental frequency of 500 kHz corresponds to a real frequency of 25 Hz, and an experimental distance of 10 mm corresponds to a real distance of 200 m, velocities as well as densities and attenuations remaining unchanged.

We performed acquisitions along Y-lines with a spatial sampling $\triangle y$ equal to 2 mm (Fig. 1(b)). The collected data thus consist of numerous parallel profiles composed of a collection of reflection data for dense grids of source-receiver locations. We process reflection data to produce seismograms corresponding to different cross-sections of the model. We pay more attention to specific profiles because they present a high interest as they cross the main structures of the model. The data collected along these profiles might thus contain reflections and diffractions from all the structures. These profiles are represented by heavy-dashed lines in Fig. 1. The seismograms are obtained after application of a low-pass filter to raw data, in order to eliminate the harmonic resonances of the transducers. Additionally, for visualization purposes, we apply a clipping procedure with different clipping numbers x to all seismograms presented below, *i.e.*, saturation of all the signals whose amplitudes are greater than x of the maximum amplitude, in order to enlighten weaker signals.

Fig. 2 shows seismograms corresponding to the acquisition line Y150 obtained with the NB and the BB transducers, respectively. Events with a time arrival smaller than 210 μs correspond to primary reflections from the top surface of the Marseille model, whereas events with greater time arrival correspond to either multiples, or reflections from the bottom surface. Noticeable discrepancies between data obtained with the two kinds of transducers can be identified in Fig. 2. More specifically, diffractions at the edges of the topographic structures can be clearly observed only on data obtained with the BB transducer. The steep slope of the fault however remains invisible whatever the transducer used. Additional experimental results obtained with both kinds of transducers can be found in [3, 5].

2.2 Numerical methods

We used two kinds of numerical methods for synthetic modeling of the zero-offset experiments : a Spectral-Element Method (SEM) and a Discretized Kirchhoff Integral Method (DKIM).

The SEM is based upon a high-order piecewise polynomial approximation of the weak formulation of the wave equation. It combines the accuracy of the pseudospectral method with the flexibility of the finite-element method [14]. In this method, the wave field is represented in terms of high-degree Lagrange interpolants, and integrals are computed based upon Gauss-Lobatto-Legendre quadrature. This combination leading to a perfectly diagonal mass matrix leads in turn

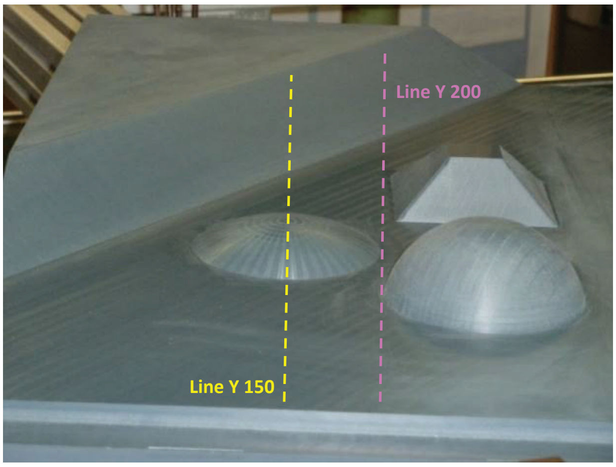

(a)

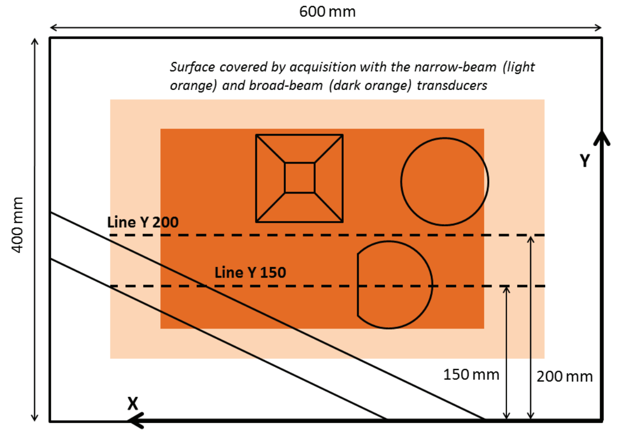

(b)

Figure 1: The Marseille model and specific acquisition lines (a), and the acquisition design (b).

to a fully explicit time scheme which lends itself very well to numerical simulations on parallel computers. It is particularly well suited to handling complex geometries and interface matching conditions [4]. The typical element size that is required to generate an accurate mesh is of the order of λ, λ being the smallest wavelength of waves traveling in the model. Very distorted mesh elements can be accurately handled. The SEM may be computationally expensive depending on the size of the domain, especially for 3D domains and high-frequency simulations. We thus mesh the model in 2D with quadrangles using the open-source software package Gmsh [8]. We implement directional directivity of standard ultrasonic transducers using a set of equidistant omnidirectional sources (like a horizontal array) whose amplitude is weighted by a Hamming window. The radiation of the simulated source is directed along the vertical. It is obtained using 51 point sources distributed over a line length of 2.54 cm, which corresponds to the diameter of the NB transducer.

The DKIM is a method based on numerical evaluation of the Kirchhoff-Helmholtz surface integral, which is a powerful tool to model the scattered wavefield from a piecewise smooth interface [15]. Both the field and its normal derivative at the interface, appearing in the integral, are commonly computed using the Kirchhoff approximation,

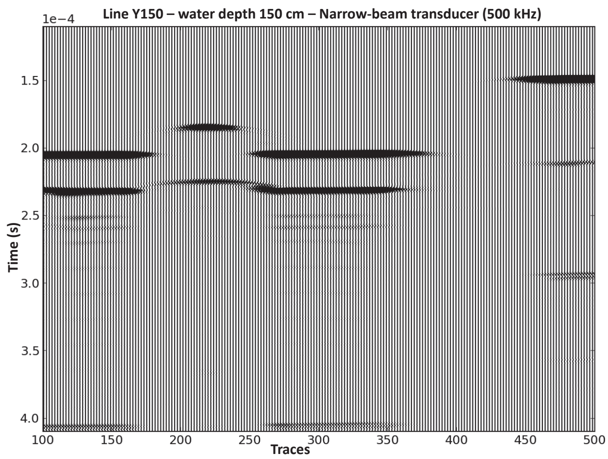

(a)

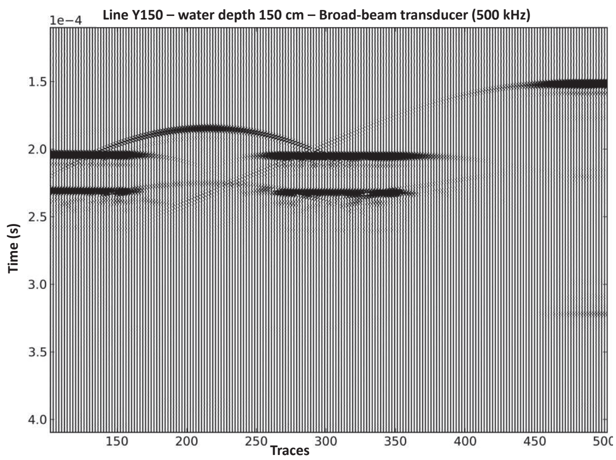

(b)

Figure 2: Laboratory zero-offset data (seismograms) obtained with the narrow-beam transducer (a), and the broad-beam transducer (b). The transducer is located at 150 mm above the Marseille model. Clipping with $x = 15$ in (a) and $x = 40$ in (b) was applied.

i.e., by multiplication of the incident wavefield and its normal derivative with the plane-wave reflection coefficient. The discretization is performed exploiting the formulas given in [1]. The detailed physical explanation of the method based on Huygens' principle is presented in [2]. Details on implementation of the method, together with the computing resources needed for simulations, can be found in [12, 13].

3 Comparison of numerical simulations with experimental data

Fig. 3 focuses on the modeling using the SEM of the wave reflection from, and transmission through, the small dome of the Marseille model illuminated by the NB transducer. Fig. 3 focuses also on the diffraction effects induced by the truncated part of the dome (Line Y150). We can notice the cuspidal form of the interaction between the wave reflections from the (flat and curved) part of the Marseille model and the wave diffractions by the truncated part or the edge of the dome. The result of the modeling of the primary reflection from the top of the PVC material along Line Y150 is shown in Fig. 4, which provides detailed comparison of two traces corresponding to two different positions of the source above the truncated dome (*i.e.*, just above the top of the dome and just above the truncated part of the dome). All datasets, including that illustrated in Fig. 4, are normalized by dividing the signal amplitude by the maximum amplitude of the whole dataset acquired for the same transducer, and we apply a static time-shift to all datasets. Visual observation of the traces shows a good fit in terms of arrival times and an acceptable fit in shape and amplitude between 2D modeled and laboratory data. Nevertheless, as the simulations using the SEM are only 2D, the influence of the 3D diffraction effect produced by the truncated part of the small dome is largely overestimated.

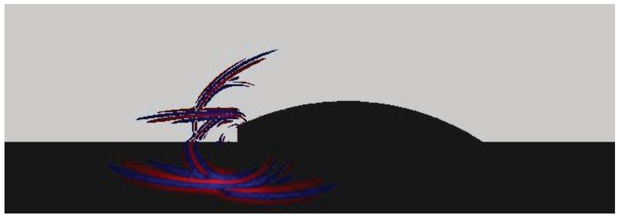

(a)

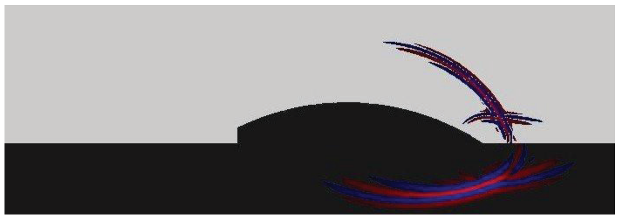

(b)

Figure 3: Numerical simulations of the wave reflections, transmissions, and diffractions in the vicinity of the truncated dome using the 2D SEM.

In Fig. 5 we show the results of modeling of the primary reflection from the top of the PVC material using the DKIM, and more specifically the single-scattering seismograms for synthetic data along Line Y200, together with the total seismograms from laboratory data obtained with the BB transducer. Direct observation of the laboratory and single-scattering seismograms shows a good fit in the modeling of reflection and diffraction events. Note that for the case of the NB transducer, its focused beam cannot illuminate the out-of-plane structures which therefore are not observed on laboratory data. On the contrary, for the case of the BB transducer, diffractions at the edges of the topographic structures and reflections from the out-of-plane structures and the fault can be clearly observed in the synthetic data, in accordance with the experimental data, even if the acquisition line does not cross the top of the structures. Though the data are zero-offset, they exhibit interesting 3D effects. Nevertheless, the steep slopes of the truncated pyramid remain invisible.

In Fig. 6 we provide a more detailed qualitative comparison of the laboratory and synthetic traces, corresponding to three chosen source positions in Fig. 5. The top trace corresponds to the reflection from the slope of the out-of-plane full dome, the flat part of the model and the slope of the out-of-plane truncated dome. The middle

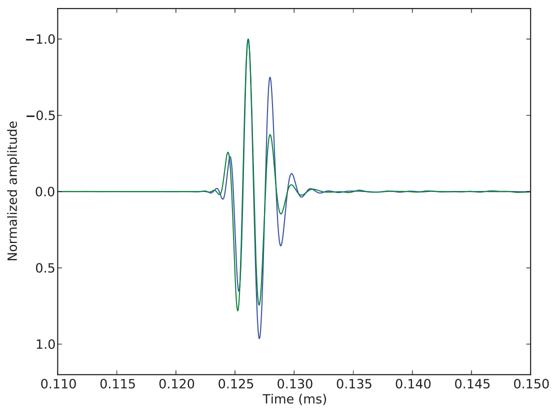

(a)

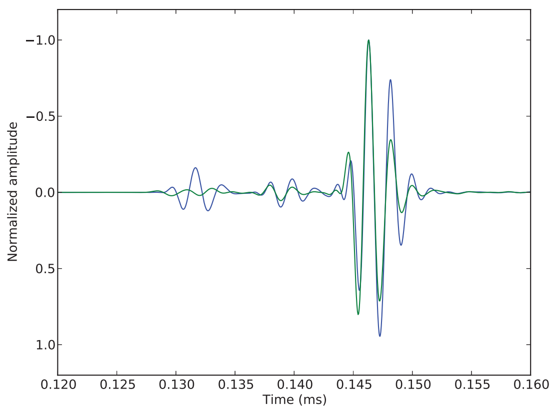

(b)

Figure 4: Comparison of the synthetic traces (blue line) obtained with 2D simulations using the SEM and laboratory traces (green line) along Line Y150, corresponding to wave reflection (a) from the top of the dome, (b) from the truncated part of the dome.

one corresponds to the reflections from the slope of the out-of-plane full dome and truncated dome, the flat part of the model and diffraction effects produced by the truncated part of the dome. The bottom one corresponds to diffraction effects produced by the fault, the reflection from the flat part of the model and diffraction effects produced by tips of the truncated pyramid. One can note a good fit of the traces in terms of the shape and the phase of the signal, but discrepancies in terms of amplitude, since the traces contain diffractions and reflections from the out-of-plane structures.

We provide a more quantitative analysis by performing a numerical comparison of these three traces selected. We use several error norms for quantitative analysis of the misfit between the synthetic and laboratory data, namely the single-valued normalized cross-correlation coefficient [16], the cross-correlation coefficient together with the root mean square (rms) misfit [6], and misfit criteria EM and PM based on the time-frequency representation using the continuous wavelet transform [10]. The single-valued normalized cross-correlation coefficient cc estimates the degree to which two signals are correlated in terms of phase and satisfies $-1 \leq cc \leq 1$. The equality $cc = 1$ is for perfect correlation, $cc = 0$ for uncorrelated series, and $cc = -1$ for negative correlation.

We provide that comparison of the misfits between the three selected laboratory and numerical traces obtained with the BB transducer in Fig. 7. The qualitative results shown above are confirmed quantitatively by the high values of the normalized cross-correlation coefficient and the low values of PM on the one hand, indicating that the phase fit is good, and by relatively high values of the rms misfit and EM on the other hand. However, the results indicate that there are phase shifts though the amplitude fit is good. The time shifts observed for the reflections from the slope of the fault are due to a possibly wrong tilt used for modeling.

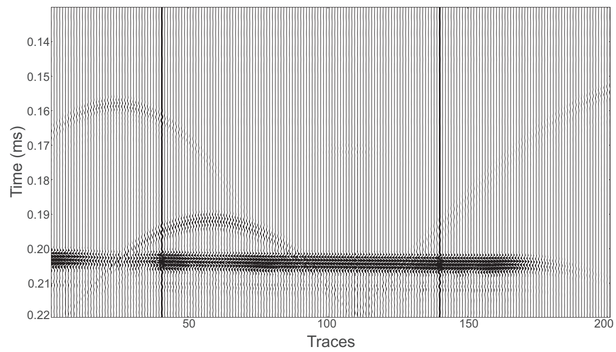

(a) Total seismogram obtained in the laboratory.

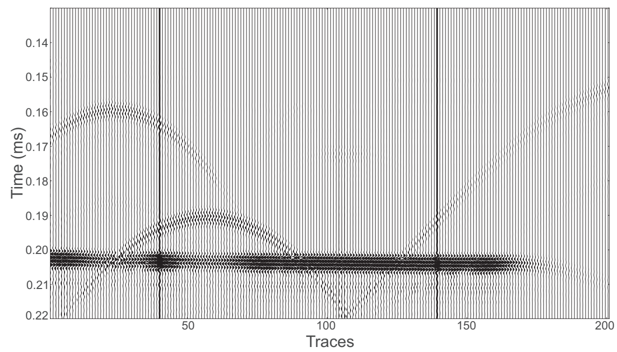

(b) Seismogram obtained with the TWSM.

Figure 5: Seismograms obtained along Line Y200.

4 Conclusion

We have tested an alternative approach for benchmarking numerical methods for 2D and 3D wave propagation. This approach consists in comparing synthetic data obtained using numerical modeling to laboratory data obtained for a known configuration. We have obtained the laboratory data by laboratory scale measurements of zero-offset reflection of broadband pulses, generated by narrow-beam and broad-beam sources, from a scaled representation of a geological model with strong 3D topographies immersed in water. The diffraction effects produced on the wavefields by the complicated features of the model, together with the existence of shadow zones, make the laboratory experiments under controlled conditions of interest. We have computed synthetic data by means of a spectral-element method and a discretized Kirchhoff integral method. The comparisons between synthetic and laboratory data exhibit a good

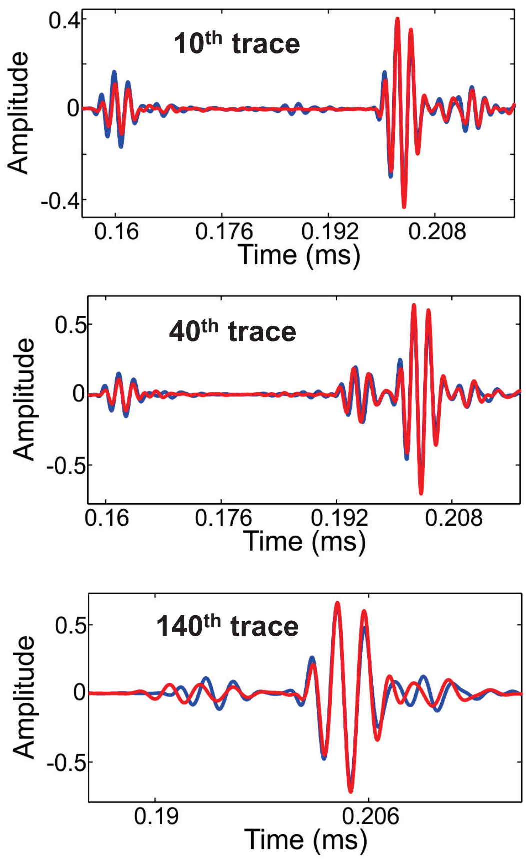

Figure 6: Comparison between laboratory (red) and numerical (blue) traces obtained with the broad-beam transducer along Line Y200 (*cf.* Fig. 5).

Traces	Normalized cross-correlation coefficient cc	Root mean square misfit rms	Single-valued envelope misfit EM	Single-valued phase misfit PM
10th	0.982	0.217	0.195	0.056
40th	0.961	0.276	0.142	0.079
140th	0.947	0.322	0.179	0.096

Figure 7: Comparison of the misfits between laboratory and numerical traces obtained with the broad-beam transducer along Line Y200, and corresponding to the three traces in Fig. 6.

qualitative and quantitative fit in terms of time arrivals and acceptable fit in amplitudes for both narrow-beam and broad-beam datasets. Nevertheless they also reveal the necessity to switch to 3D in future work and use our numerical tools to model 3D zero-offset wave reflection from strong topographic structures and to better describe the reflection phenomena with more complex reflection coefficients.

The data sets obtained during this measurement campaign seem promising for future use as a real-data benchmark for 2D and 3D model comparisons. The next step will consist in a multi-offset experiment with broad-beam transducer. In future work we plan to perform numerical cross-validation of 2D and 3D numerical methods and techniques on the obtained data in order to analyze the respective limitations of each method and to choose the right strategy for further development of the methods. This is the final goal of our project called BENCHIE (http://www.benchie.cnrs-mrs.fr/).

Acknowledgements

We thank the INSIS Institute of the French CNRS, Aix-Marseille University, the Carnot Star Institute, the VISTA Project and the Norwegian Research Council through the ROSE Project for financial support. We greatly acknowledge Stephan Devic (previously at LMA Marseille) for carving the Marseille model.

References

[1] M. A. Ayzenberg, A. M. Aizenberg, H. B. Helle, K. D. Klem-Musatov, J. Pajchel, and B. Ursin. 3D diffraction modeling of singly scattered acoustic wavefields based on the combination of surface integral propagators and transmission operators. *Geophysics*, 72(5):SM19–SM34, 2007.

[2] M. A. Ayzenberg, A. M. Aizenberg, and B. Ursin. Tip-wave superposition method with effective reflection and transmission coefficients: A new 3D Kirchhoff-based approach to synthetic seismic modeling. *The Leading Edge*, 28:582–588, 2009.

[3] P. Cristini, N. Favretto-Cristini, A. Tantsereva, B. Ursin, A.M. Aizenberg, and D. Komatitsch. Laboratory benchmarks vs. synthetic modeling of seismic wave propagation in complex environments (BENCHIE project): Results for a Spectral-Element Method and the Tip-Wave Superposition Method. In *Proceedings of Meetings on Acoustics*, volume 17, page 070024, 2012.

[4] P. Cristini and D. Komatitsch. Some illustrative examples of the use of a Spectral-Element Method in ocean acoustics. *Journal of the Acoustical Society of America*, 131(3):EL229–EL235, 2012.

[5] N. Favretto-Cristini, A. Tantsereva, P. Cristini, B. Ursin, D. Komatitsch, and A.M. Aizenberg. Numerical modeling of zero-offset laboratory data in a strong topographic environment : results for a spectral-element method and a discretized Kirchhoff integral method. *Earthquake Science (in press)*, 2014.

[6] M. Fehler and P.J. Keliher. *SEAM Phase I: Challenge of subsalt imaging in Tertiary basins, with emphasis on deepwater Gulf of Mexico*. SEG, 2011.

[7] W. S. French. 2D and 3D migration of model-experiment reflection profiles. *Geophysics*, 39(3):265–277, 1974.

[8] C. Geuzaine and J.-F. Remacle. Gmsh: a three-dimensional finite-element mesh generator with built-in pre- and post-processing facilities. *International Journal for Numerical Methods in Engineering*, 79(11):13091331, 2009.

[9] M. Houbiers, E. Wiarda, J. Mispel, D. Nikolenko, D. Vigh, B.-E. Knudsen, M. Thompson, and D. Hill. 3D full-waveform inversion at Mariner : a shallow North Sea reservoir. In *SEG Technical Program Expanded Abstracts 2012*, 2012.

[10] M. Kristeková, J. Kristek, and P. Moczo. Time-frequency misfit and goodness-of-fit criteria for quantitative comparison of time signals. *Geophysical Journal International*, 178:813–825, 2009.

[11] P. Moczo, J.-P. Ampuero, J. Kristek, S.M. Day, M. Kristeková, P. Pazak, M. Galis, and H. Igel. Comparison of numerical methods for seismic wave propagation and source dynamics the SPICE code validation. In *International Symposium on the Effects of Surface Geology on Seismic Motion 3*, 2006.

[12] A. Tantesereva, B. Ursin, N. Favretto-Cristini, P. Cristini, and A.M. Aizenberg. Numerical modeling of three-dimensional zero-offset laboratory data by a discretized Kirchhoff integral. *Geophysics (in press)*, 2014.

[13] A. Tantsereva, B. Ursin, N. Favretto-Cristiniand P. Cristini, D. Komatitsch, and A. M. Aizenberg. Numerical modeling of zero-offset acoustic data by the Tip-Wave Superposition Method. In *P75th Conference & Exhibition , EAGE*, 2013.

[14] J. Tromp, D. Komatitsch, and Q. Liu. Spectral-Element and Adjoint Methods in Seismology. *Communications in Computational Physics*, 3(1):1–32, 2008.

[15] M. Tygel and B. Ursin. Weak-contrast edge and vertex diffractions in anisotropic elastic media. *Wave Motion*, 29:363373, 1999.

[16] D.S. Wilks. *Statistical methods in the atmospheric science, 3 ed.* Academic Press, 2011.